Korean J. Chem. Eng., 35(3), 764-769 (2018)
DOI: 10.1007/s11814-017-0334-4

pISSN: 0256-1115
eISSN: 1975-7220

Rapid solvothermal synthesis of microporous UiO-66 particles for carbon dioxide capture

Sunyoung Bae*, Nabilah Zaini, Khairul Sozana Nor Kamarudin***, Kye Sang Yoo****, Jinsoo Kim*,†, and Mohd Roslee Othman**,†**

*Department of Chemical Engineering, Kyung Hee University, Global Campus, 1732 Deogyeong-daero, Giheung-gu, Yongin-si, Gyeonggi-do 17104, Korea
**School of Chemical Engineering, Universiti Sains Malaysia, 14300 Nibong Tebal, Penang, Malaysia
***Chemical Process Engineering Department, Malaysia-Japan International Institute of Technology, Universiti Teknologi Malaysia Kuala Lumpur, 54100 Wilayah Persekutuan Kuala Lumpur, Malaysia
****Department of Chemical and Biomolecular Engineering, Seoul National University of Science and Technology, Seoul 01811, Korea

(*Received 29 September 2017 • accepted 1 December 2017*)

Abstract−One of the important metal-organic frameworks known as UiO-66 has received significant attention recently due to its unprecedented chemical and thermal stability, with exceptionally high surface area. We prepared UiO-66 particles by a rapid solvothermal method which took only 30 min at 120 °C to prepare, compared to the previous work which took longer than 12 h. Changing the precursor's concentration ratio from 0.5 to 1.5 and reaction temperature from 80 °C to 140 °C resulted in the increase of UiO-66 particle size from 30 to 150 nm. The highest surface area of ca. 1,300 m^2/g was achieved at concentration ratio of 1 and temperature of 120 °C with bi-modal pore sizes of ca 0.60 nm and 1.25 nm, respectively. The UiO-66 particles with the highest surface area were then employed to capture carbon dioxide from a binary gas mixture. Results from CO_2 adsorption capacity measurement using UiO-66 indicate that the adsorbent was capable of capturing 1.3611 mmol/g at pressure of 1.5-1.7 bar and flowrate of 300 cm^3/min.

Keywords: UiO-66, Zr-MOF, Gas Separation, Carbon Dioxide, Sol-gel, Adsorption

INTRODUCTION

Metal-organic frameworks (MOFs) are hybrid crystalline materials composed of metal ions or clusters coordinated to organic ligands to form nanoporous structures [1,2]. MOFs have attracted wide attention due to their remarkable properties such as controllable pore structures and high surface areas which show potential applications in gas storage, gas separation, chemical sensing, heterogeneous catalysis [3-11]. Among the MOFs, UiO-66 has attracted more attention recently due to its unprecedentedly high thermal and chemical stability. UiO-66 consists of a $Zr_6O_4(OH)_4$ octahedron that is linked 12 times to the adjacent octahedral via a 1,6-benzene-dicarboxylate (BDC) linker to form a highly packed fcc structure. Its dense structure possesses two different types of pore, octahedral (11 Å) and tetrahedral (8 Å), accessible through windows of ca. 6 Å [12].

Different MOF synthesis methods have been applied in the last 20 years. Traditionally, MOF has been prepared at room temperature with extremely long synthesis time to develop its structure. Alternatively, methods such as conventional electric (CE) heating, microwave (MW) heating, electrochemistry (EC), mechanochemistry (MC), and ultrasonic (US) have been attempted to overcome the weakness. Likewise, numerous procedures for the synthesis of UiO-66 have been reported. Most processes involve solvothermal synthesis at temperatures of 80-120 °C, typically over 24 hours [13-20]. In this study, we introduced a rapid solvothermal method which took only 30 min at 120 °C to complete the synthesis and obtain the UiO-66 particles. We also addressed the effect of varying concentration of precursors and reaction temperature on the physical characteristics of the resulting UiO-66. The UiO-66 sample was then tested to determine the carbon dioxide (CO_2) adsorption capacity and its potential as adsorbent in carbon capture.

EXPERIMENT

1. Solvothermal Synthesis of UiO-66

All chemicals were obtained commercially (Aldrich) and used without further purification. For typical synthesis, 1.06 g of zirconium (IV) chloride ($ZrCl_4$) and 0.78 g of 1,4 benzenedicarboxylic acid (BDC) were dissolved separately, each in 30 ml dimethylformamide (DMF). The product sample prepared with original recipe (concentration ratio of 1) was denoted as UiO-66 conc×1. The amounts of $ZrCl_4$ and BDC were controlled to half (concentration ratio of 0.5) and double (concentration ratio of 2) of the original amount in the same volume of solvent. The two product samples were denoted as UiO-66 conc×0.5 and UiO-66 conc×2, respectively. The two solutions were mixed completely after adding 2 ml of de-ionized water and then the mixture was transferred into a

†To whom correspondence should be addressed.
E-mail: jkim21@khu.ac.kr, chroslee@usm.my
Copyright by The Korean Institute of Chemical Engineers.

Teflon-lined stainless-steel autoclave. The autoclave was placed in an oil bath at different temperature of 80 °C, 100 °C, 120 °C and 140 °C for 30 min. After the solution was cooled to room temperature in air for 2 h, the resulting UiO-66 particles were separated via centrifugation and washed several times with ethanol. Finally, the particles were dried at 70 °C overnight.

2. Characterization

The XRD equipment (M18XHF-SRA, Mac Science, Japan) was used to identify the crystal phases of UiO-66 samples at narrow angle between 2° and 40° in 0.05 step size at a scanning rate of 1°/min using Cu Kα radiation (k=1.5406 Å), with accelerating voltage and current of 40 kV and 40 mA, respectively. The morphology and textural details of the samples were observed by a field-emission scanning electron microscope (FE-SEM model Leo-Supra 55, Carl Zeiss STM, Germany). The N_2 adsorption-desorption isotherms at 77 K were measured with a Belsorp-max instrument (BEL Japan Inc., Japan). The Brunauer-Emmet-Teller (BET) surface area was calculated using the BET model in the linear region and pore size distributions were calculated using the NLDFT method.

3. CO_2 Capture

CO_2 (99.999%) adsorption was performed using adsorption equipment as depicted in Fig. 1(a). Approximately, 3.5 g of UiO-66 sample was placed in the middle of the column. The UiO-66 was sandwiched between glass wool and molecular sieve to prevent the adsorbent from leaking out of the bed and to remove moisture in the feed gas stream, respectively. The unit is connected to a gas chromatograph (Agilent 7820A) for gas analysis. In performing CO_2 adsorption experiment at room temperature, the flow rate, initial pressure, adsorption time and final pressure were set at 300 cm^3/min, 1.5 bar and 5 min respectively. During breakthrough experiment, the pressure was locked at 1.5 bar, but it was gradually increased to 2.0 bars and then decreased before it finally maintained at 1.7 bars (Fig. 1(b)).

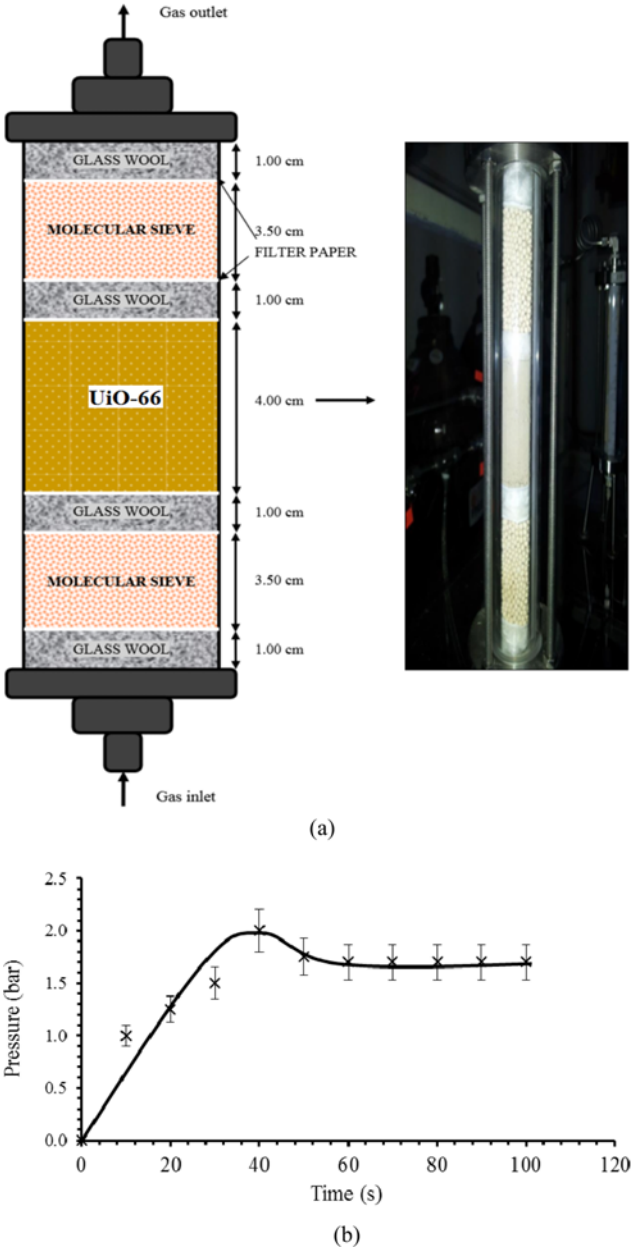

Fig. 1. Schematic of adsorption column showing (a) position of UiO-66 sample, (b) breakthrough pressure with time.

RESULTS AND DISCUSSION

Fig. 2 shows XRD patterns of the UiO-66 synthesized at different concentration ratios and constant temperature of 120 °C. UiO-66 conc×1 sample synthesized using typical precursor concentration showed the highest intensity peak, and therefore exhibited the maximum level of crystallinity, whereas UiO-66 conc×0.5 sample showed the lowest level of crystallinity. UiO-66 conc×2 sample indicated moderate level of crystallinity. The level of concentration did not seem to follow a specific trend, possibly due to the synergetic balance of precursors that was needed in the formation of UiO-66 crystals. In achieving the synergy, the $Zr_6O_4(OH)_4$ inner core that was initially a regular highly packed face-centered cubic structure was thought to undergo a continuum of truncations into the finally rectified form of a polyhedron during nucleation and

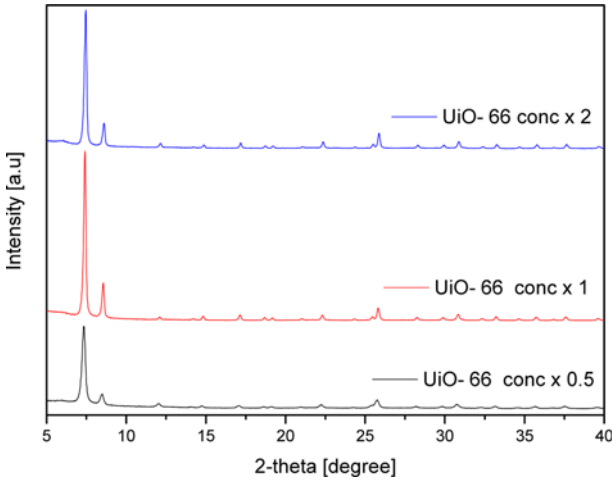

Fig. 2. XRD patterns of the UiO-66 synthesized with different precursor concentration ratio at temperature 120 °C.

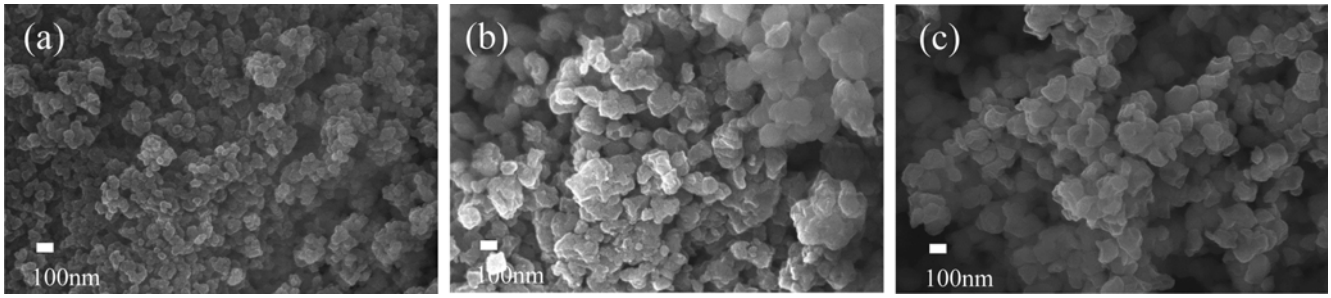

Fig. 3. SEM images of the UiO-66 synthesized at temperature 120 °C with different precursor concentration ratio, (a) 0.5, (b) 1, and (c) 2.

crystal growth. The edges of this polyhedron were then bridged by the carboxylates originating from the dicarboxylic acid, while Zr atom was bonded with the ligands through oxygen atom supplied by the carboxylates.

The FE-SEM images of UiO-66 samples with various precursor concentrations are shown in Fig. 3. The morphology of the samples was affected by the ratio of the precursors used. The particle species should ideally exhibit a topology of a regular octahedron or dual polyhedron of a cube which is a rectified tetrahedron. However, the image of UiO-66 conc×0.5 sample observed here hardly revealed the regular UiO-66 geometry, possibly due to some perturbation during the synthesis or incomplete truncation of the particle species into the final rectified octahedron or a perfectly three-dimensional cross polytope in the presence of water (since de-ionized water was used during the synthesis). Another factor that affects the geometry and size of particles is solubility change. The growth of primary particles in a particulate sol is normally assisted by a phenomenon where the particles grow and decrease in number as highly soluble small particles dissolve and re-precipitate on a less soluble one. For a particle having a negative curvature (radius of the neck is negative), its solubility is lower than that of the particle having positive curvature. Therefore, the latter tends to precipitate on the surface of the former, leading to growing of the particle's neck that strengthens the particle-particle cluster during agglomeration [22]. As observed from the SEM images, it is obvious that the particles agglomerated and increased in size as the concentration ratio was increased from 0.5 to 1.5 due to the solubility change.

The pore size distributions of the samples synthesized with various precursor concentrations are shown in Fig. 4. All three samples exhibited two distinct (bi-modal) mean pore sizes. UiO-66 conc×1 exhibited the narrowest distribution and smallest mean pore sizes of ca 0.60 nm and 1.25 nm, respectively, followed by UiO-66 conc×2 with bi-modal pore sizes of ca 0.65 nm and 1.20 nm, respectively, and UiO-66 conc×0.5 with bi-modal pore sizes of ca 0.80 nm and 1.20 nm, respectively. This result is in a good agreement with XRD analysis and SEM results as discussed earlier.

Fig. 5 shows the XRD patterns of UiO-66 conc×1 samples prepared at different solvothermal temperatures. The results reveal that the samples were highly crystalline with the main intensity peaks (the characteristic of UiO-66) appearing at 2θ of 7.4°, 8.5° and 25.5°. In fact, the samples prepared in this work appear to be more crystalline than the samples reported in the literature, where three different ligands such as 2-amino-benzenedicarboxylic acid, 2-nitro-benzenedicarboxylic acid and 2-bromo-benzenedicarboxylic acid were used to add the functionality [16]. The peak intensity of the samples increased with increasing synthesis temperature of up to 120 °C. Although increasing peak intensity is expected at higher temperature, increasing the synthesis temperature further to 140 °C

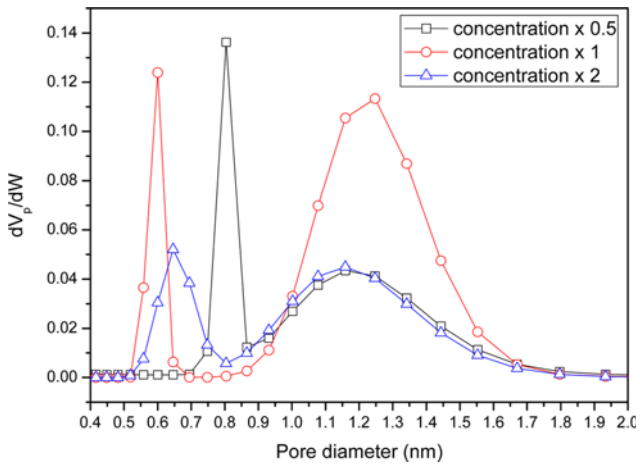

Fig. 4. Pore size distribution of the UiO-66 synthesized with different precursor concentration ratio at temperature 120 °C.

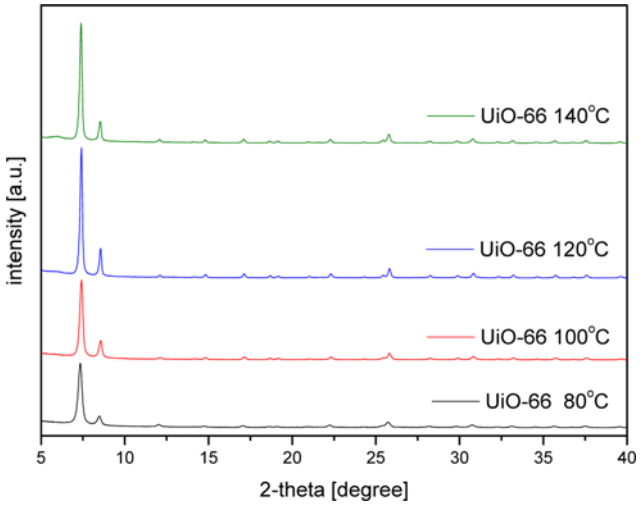

Fig. 5. XRD patterns of the UiO-66 synthesized with different temperature at precursor concentration ratio of 1.

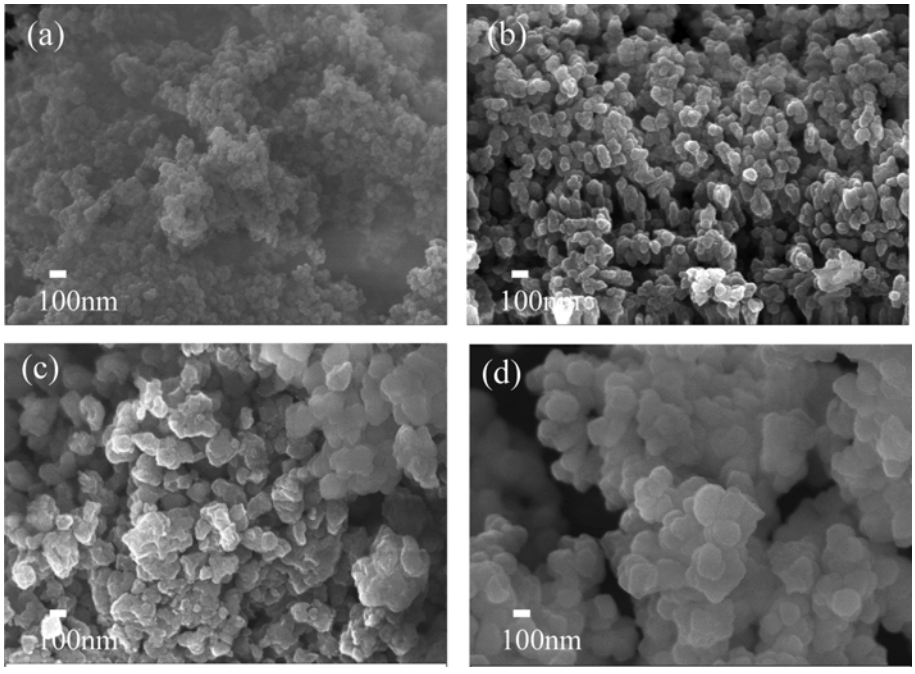

Fig. 6. SEM images of the UiO-66 synthesized at precursor concentration ratio of 1 with different temperature (a) 80 °C, (b) 100 °C, (c) 120 °C, and (d) 140 °C.

resulted in more or less similar peak's intensity with the sample at 120 °C.

The morphology of UiO-66 prepared with various synthesis temperatures is shown in Fig. 6. From the SEM images, the size of particles increased as the temperature was increased from 80 °C to 140 °C. Moreover, the shape of sample was well formed with increasing synthesis temperature. At high temperature and low pressure conditions, the solubility of the colloid system typically increases, thereby facilitating further growth of the particle [21]. For a particle precursor sol that exhibits a positive curvature, the smaller size particle has higher solubility and lower density than that of the larger particle. Therefore, the smaller particle tends to dissolve and pre-

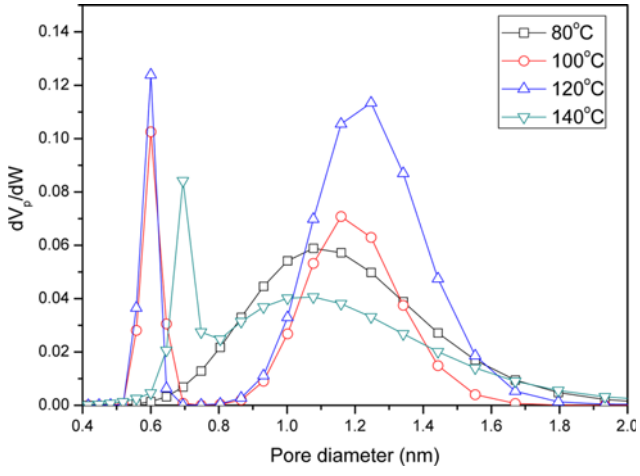

Fig. 7. Pore size distribution of the UiO-66 synthesized with different temperature at precursor concentration ratio of 1.

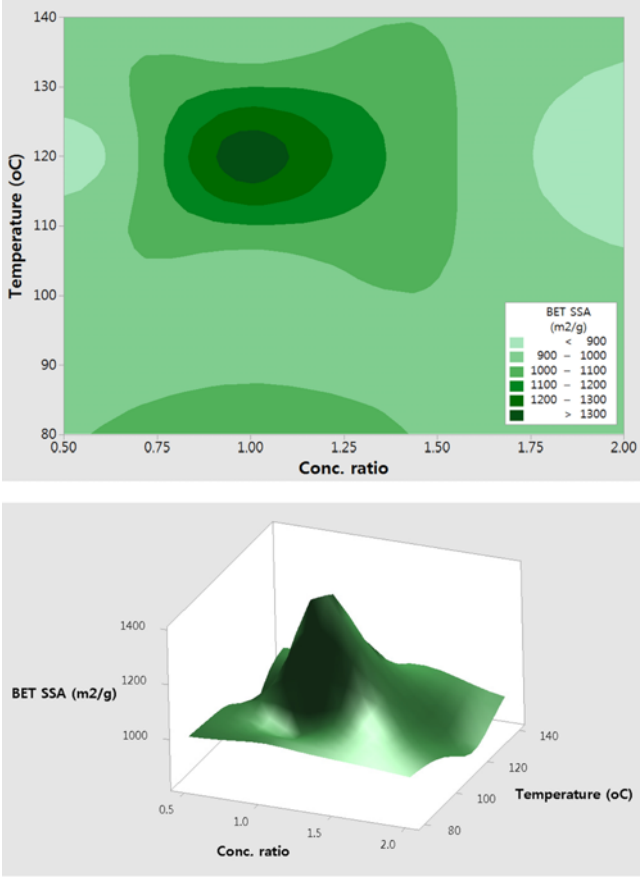

Fig. 8. Surface and contour plot of the optimum synthesis conditions of UiO-66 (concentration ratio of 1 and synthesis temperature of 120 °C).

cipitate on the surface of the larger size particle to form a growing particle that only ceases to grow when the solubility difference becomes extremely small [22]. The pore size distribution of the samples with various synthesis temperatures was measured as shown in Fig. 7. Although the effect of the temperature on pore size did not seem to change much from Fig. 4 with respect to bi-modality of pores, the synthesis temperature at 120 °C gave the most narrow pore size distribution, which is consistent with the XRD analysis on the crystallinity level.

The effect of reaction temperature and precursor concentration on BET surface areas of UiO-66 was analyzed using the statistical secondary reaction surface morphology. The optimal reaction conditions were determined according to BET specific surface area of UiO-66, which is representative of MOF synthesis performance. UiO-66 with the highest surface areas was synthesized under the synthesis temperature of 120 °C and original precursor concentration (ratio of 1). The optimal conditions for the surface area under the above conditions are shown using surface and contour maps. As shown in Fig. 8, the optimal synthesis conditions of UiO-66 with various specific surface areas are presented in all ranges.

Fig. 9(a) shows a plot of the ratio C/Co (outlet CO_2 concentration/feed CO_2 concentration) as a function of the adsorption time. Breakthrough occurred when CO_2 started to emerge at the exit bed section at 5% from its feed concentration [23]. The breakthrough curve from the figure indicates that the adsorption time should be taken at 3-5 minutes, and complete saturation (CO_2 completely filled up the pores in the bed) was achieved at approximately 10 minutes. Note that UiO-66 sample is close to an ideal situation with negligible mass-transfer resistance in which there is no axial dispersion. The closer the breakthrough to the ideal condition, the more efficient is the mass transfer zone [23]. The figure also compares a horizontally stretched breakthrough curve of *Kenaf* activated carbon (AC), which deviates from the ideality and is characterized by dispersion. Fig. 9(b) shows the decreasing adsorption capacity when the adsorbent was reused for the following adsorption cycles. It seems that regeneration of UiO-66 would still be necessary to maintain the adsorption capacity of the adsorbent and purity of the product gas. Results from CO_2 adsorption reveal that UiO-66 sample from this work performed comparatively well with the other commercialized AC adsorbent in the market with adsorption capacity of 1.311 mmol CO_2 per gram of UiO-66. However, Zr-MOF embedded with graphene oxide (GO) [24] and UiO-66 reported previously which employed a longer solvo-thermal process of 24 h, immersion time of 5 d and vacuumed drying of 48 h [25] outperform the current sample with adsorption capacity reaching 3.37 mmol/g and 2.27 mmol/g, respectively. Nevertheless, the previous samples required an additional compound (GO) and longer synthesis time, respectively, to achieve high CO_2 adsorption.

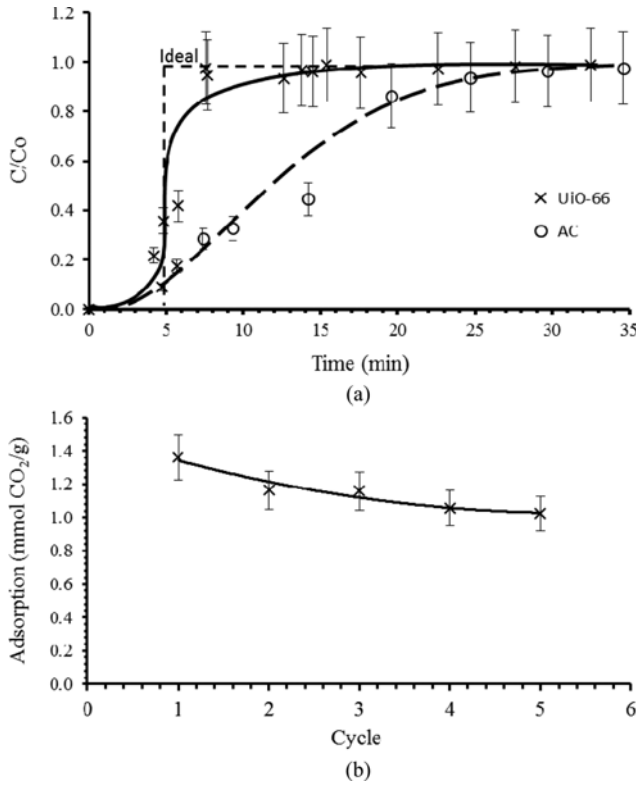

Fig. 9. Dynamics of UiO-66 through (a) breakthrough curve, (b) adsorption cycle.

CONCLUSION

The UiO-66 prepared using the method proposed in this paper was found to be favorable for deployment in industry due to shortened route of synthesis. The UiO-66 is suitably used as a support for catalysis and adsorption in the separation application due to its unprecedented stability and exceptionally high surface area. The physical properties of UiO-66 can also be engineered by changing the precursor concentration or reaction temperature. Despite lower CO_2 adsorption performance than the previously synthesized and modified Zr-MOF materials, UiO-66 prepared from this work performed comparatively well with the other commercialized adsorbent in the market with CO_2 adsorption capacity of 1.311 mmol/g. It is expected that the performance would be improved tremendously if UiO-66 were to be embedded with CO_2 highly affinitive materials.

ACKNOWLEDGEMENTS

This work was supported by the Fundamental Research Grant Scheme (FRGS) for Geran Sanjungan Penyelidikan (GSP), Ministry of Higher Education (MOHE), Malaysia and the National Research Foundation of Korea (NRF) (NRF-2017M1A2A2043451 and NRF-2016R1A2B4014805) funded by the Ministry of Science and ICT of Korea.

REFERENCES

1. H. C. Zhou, J. R. Long and O. M. Yaghi, *Chem. Rev.*, **112**, 673 (2012).
2. H. Furukawa, K. E. Cordova, M. O'Keeffe and O. M. Yaghi, *Science*, 341 (2013).
3. L. J. Murray, M. Dincă and J. R. Long, *Chem. Soc. Rev.*, **38**, 1294 (2009).
4. J. Sculley, D. Yuan and H.-C. Zhou, *Energy Environ. Sci.*, **4**, 2721 (2011).

5. J.-R. Li, R. J. Kuppler and H.-C. Zhou, *Chem. Soc. Rev.*, **38**, 1477 (2009).
6. J. An, S. J. Geib and N. L. Rosi, *J. Am. Chem. Soc.*, **132**, 38 (2010).
7. Y.-S. Bae, A. M. Spokoyny, O. K. Farha, R. Q. Snurr, J. T. Hupp and C. A. Mirkin, *Chem. Commun.*, **46**, 3478 (2010).
8. K. Farha, A. M. Shultz, A. A. Sarjeant, S. T. Nguyen and J. T. Hupp, *J. Am. Chem. Soc.*, **133**, 5652 (2011).
9. L. Ma, C. Abney and W. Lin, *Chem. Soc. Rev.*, **38**, 1248 (2009).
10. L. E. Kreno, K. Leong, O. K. Farha, M. Allendorf, R. P. VanDuyne and J. T. Hupp, *Chem. Rev.*, **112**, 1105 (2012).
11. M. D. Allendorf, C. A. Bauer, R. K. Bhakta and R. J. T. Houk, *Chem. Soc. Rev.*, **38**, 1330 (2009).
12. J. H. Cavka, S. Jakobsen, U. Olsbye, N. Guillou, C. Lamberti, S. Bordiga and K. P. A. Lillerud, *J. Am. Chem. Soc.*, **130**, 13850 (2008).
13. P. M. Schoenecker, G. A. Belancik, B. E. Grabicka and K. S. Walton, *AIChE J.*, **59**, 1255 (2012).
14. S. Biswas and P. Van Der Voort, *Eur. J. Inorg. Chem.*, 2154 (2013).
15. J. B. DeCoste, G. W. Peterson, H. Jasuja, T. G. Glover, Y.-G. Huang and K. S. Walton, *J. Mater. Chem. A*, **1**, 5642 (2013).
16. M. Kandiah, M. H. Nilsen, S. Usseglio, S. Jakobsen, U. Olsbye, M. Tilset, C. Larabi, E. A. Quadrelli, F. Bonino and K. P. Lillerud, *Chem. Mater.*, **22**, 6632 (2010).
17. H. Wu, T. Yildirim and W. Zhou, *J. Phys. Chem. Lett.*, **4**, 925 (2013).
18. A. Schaate, P. Roy, A. Godt, J. Lippke, F. Waltz, M. Wiebcke and P. Behrens, *Chem.-Eur. J.*, **17**, 6643 (2011).
19. V. Guillerm, F. Ragon, M. Dan-Hardi, T. Devic, M. Vishnuvarthan, B. Campo, A. Vimont, G. Clet, Q. Yang, G. Maurin, G. Fe´rey, A. Vittadini, S. Gross and C. Serre, *Angew. Chem.*, **51**, 9267 (2012).
20. Y. Huang, W. Qin, Z. Li and Y. Li, *Dalton Trans.*, **41**, 9283 (2012).
21. D. J. S. Birch and C. D. Geddes, *Chem. P. Lett.*, **320**, 229 (2000).
22. J. W. Lee, M. R. Othman, T. G. Lee, W. S. Kim and J. Kim, *Micropor. Mesopor. Mater.*, **116**, 561 (2008).
23. A. D. Wiheeb, Z. Helwani, J. Kim and M. R. Othman, *Sep. Purif. Rev.*, **45**, 108 (2016).
24. Y. Cao, Y. Zhao, Z. Lv, F. Song and Q. Zhong, *J. Ind. Eng. Chem.*, **27**, 102 (2015).
25. H. R. Abid, H. Tian, H. M. Ang, M. O. Tade, C. E. Buckley and S. Wang, *Chem. Eng. J.*, **187**, 415 (2012).